Journal of Materials Chemistry C

PAPER

View Article Online
View Journal | View Issue

Cite this: J. Mater. Chem. C, 2014, 2, 9215

Superspace application on magnetic structure analysis of the Pb_2MnWO_6 double perovskite system

Fabio Orlandi,*[a] Lara Righi,[ad] Clemens Ritter,[b] Chiara Pernechele,[c] Massimo Solzi,[c] Riccardo Cabassi,[d] Fulvio Bolzoni[d] and Gianluca Calestani[ad]

Received 4th July 2014
Accepted 7th September 2014

DOI: 10.1039/c4tc01450b

www.rsc.org/MaterialsC

The commensurate crystal structure of the magnetic phase occurring below 7 K of the multiferroic Pb_2MnWO_6 perovskite has been solved by the introduction of the superspace approach. This lead based double perovskite is characterized by a complex ferrielectric non-centrosymmetric nuclear structure with orthorhombic symmetry stable in a wide temperature range. As indicated from the analysis of powder neutron diffraction data, the low temperature antiferromagnetic structure showing a propagation vector $\kappa = [1/4\ 0\ 0]$ is stabilized by a multi-step process involving the evolution from incommensurate to commensurate spin ordering with a concomitant change of the magnetic symmetry. The determination of the Pb_2MnWO_6 magnetic structure offers a meaningful example of the superspace application and provides a detailed phase diagram of the involved magnetic states. Nowadays this ordered perovskite could be considered as a new type of multiferroic material combining ferrielectric properties and a long period antiferromagnetic structure.

Introduction

The superspace approach is generally recognized as the standard method to solve and analyse commensurate and incommensurate crystal modulated structures. However, modulation can be observed in magnetic structures as well, and the application of superspace to these cases, suggested at the initial stage of its formulation by Janner and Janssen,[1] has been described in few published works.[2–5] The relevance in adopting superspace for the study of magnetically ordered structures is represented by the complete determination of the global symmetry of the system (in terms of magnetic and nuclear contribution) expressed with crystallographic rules. In recent years, the development of the Jana2006 software has provided a useful tool extending the application of the superspace formalism to the magnetic structure analysis.[6]

The superspace method can furthermore also be adapted to the analysis of commensurate magnetic structures, which are the most frequent case in solid state physics, and possible magnetic transitions involving different spin arrangements, *i.e.* from incommensurate to commensurate ordering, can be straightforwardly monitored. If the structural investigation involves correlated systems such as multiferroic materials, the knowledge of the point symmetry of the magnetic structure assumes a fundamental significance for the study of the tensor property ruling the magneto–electric interaction.[7]

In this paper we illustrate the successful application of superspace formalism to the determination and analysis of the low temperature magnetic structure of the lead based double perovskite Pb_2MnWO_6 (PMW). This system, considered as a promising multiferroic material,[8] possesses a polar active Pb^{2+} ion, which is classically characterized by a non-centrosymmetric environment, related to the $6s^2$ lone pair and strong Pb–O hybridization, and a magnetic Mn^{2+} responsible for the magnetic transition with the critical temperature close to 44 K. From single crystal diffraction data it has been found that, different to what is reported in the literature,[9] the orthorhombic space group of PMW at room temperature is the non-centrosymmetric $Pmc2_1$.[8] The electric properties of this perovskite are generated from the electronic instability of the Pb^{2+} coordination constituting a complex ferrielectric structure at RT.[8] Concerning the magnetic properties, magnetization measurements *versus* temperature reveal, besides a first transition at 44 K, a second change of magnetic properties near to 9 K. Although the structural and electrical properties of PMW are reported in the literature[9] no detailed investigation has been carried out in order to determine the type of magnetic interaction occurring at 44 K. Here we describe the structural analysis of the magnetic phase transitions using neutron powder diffraction paying special attention to the symmetry of the system. The detailed insights obtained from the determination of the magnetic

[a]Dipartimento di Chimica, Università di Parma, Parco Area delle Scienze 17/A, 43124 Parma, Italy. E-mail: fabio.orlandi@nemo.unipr.it
[b]Institute Laue-Langevin, Boite Postale 156, F-38042, Grenoble, France
[c]Dipartimento di Fisica e Scienze della Terra, Università di Parma, Parco Area delle Scienze 7/A, 43124 Parma, Italy
[d]IMEM-CNR, Parco Area delle Scienze 37/A, 43124 Parma, Italy

structure of PWM and its temperature dependence evidence the presence of a possible magneto-striction effect indicative of a direct magneto–electric coupling.

Experimental Section

A ceramic Pb_2MnWO_6 sample was synthesized by solid-state reaction following a previously reported procedure.[9] Stoichiometric amounts of PbO, $MnCO_3$ and WO_3 were ground, heated at 800 °C at 180 °C h^{-1} and then fired at this temperature for 2 h in an N_2 stream. The obtained powder was re-ground, pressed into pellets and sintered at 820 °C for 4 h. The phase purity was checked by powder X-ray diffraction (PXRD) by using a Thermo ARL X'tra diffractometer equipped with Cu Kα radiation and a Si(Li) Thermo Electron solid-state detector to eliminate the fluorescence of manganese.

The magnetic characterization was performed by means of a SQuID magnetometer (MPMS XL Quantum Design, maximum applied field of 50 kOe) in the temperature range 4–300 K. In particular Zero Field Cooling (ZFC) and Field Cooling (FC) curves were measured with different applied fields (H = 50 Oe, 500 Oe, 1 kOe and 5 kOe). Moreover $M(H)$ curves were measured at 3 and 25 K in the range ±50 kOe.

Neutron powder diffraction data were collected at the Institute Laue-Langevin (Grenoble, France) on the high-resolution diffractometer D2B (λ = 1.594 Å) and the high intensity diffractometer D20 (λ = 2.41 Å). D2B data were collected at 2 K whereas the thermal evolution of the diffraction pattern was followed at the D20 line in the range 2–300 K. The refinement of nuclear and magnetic structures was carried out with the Jana2006 software.[6]

Results

Magnetic measurements

Magnetic susceptibility measurements showed that, with decreasing temperature, the system presents two critical temperatures at T_1 = 44 K and T_2 = 9 K, as shown in Fig. 1. The Curie–Weiss fit of the paramagnetic region of the inverse susceptibility reveals an antiferromagnetic (AF) nature of the interaction between the magnetic ions ($\Theta_{C-W} = -24.3 \pm 0.1$ K) and a moment μ_{eff} = 5.7 μ_B in agreement with Mn^{2+} ions in high spin configuration with quenched orbital momentum. Despite the AF magnetic interaction, the system shows a weak ferromagnetism (FM) evidenced by the irreversibility between ZFC and FC measurements.

An interesting field dependence of the ZFC–FC curves is observed (Fig. 2) by increasing the applied field in the $M(T)$ measurements. In particular, while the 9 K transition remains evident for all the applied fields, the 44 K one is strongly reduced by increasing the applied field and is no longer evident for H = 5 kOe. For the highest applied field, no more irreversibility between the ZFC and the FC curve is present. Moreover, by considering the effect of the applied field on the mass susceptibility at low temperature in the FC curves, the value of the χ_m at 9 K decreases and it is almost halved by increasing the applied field from 50 Oe to 5 kOe. This effect is still present, albeit strongly reduced, in the ZFC measurements as it can be inferred from Fig. 2.

The hysteresis loops measured at 25 and 3 K are shown in Fig. 3. In spite of a weak FM (a small opening of the loop with H_c = 160 Oe is detected in both cases) the predominant linear character of the response is a further indication of the AF nature of the transitions.

Magnetic structure analysis

PMW was reported, by single crystal XRD,[8] to crystallize in an orthorhombic $Pmc2_1$ perovskite superstructure, related to the primitive cell by the relationship $a = 2a_p$, $b = \sqrt{2}a_p$ and

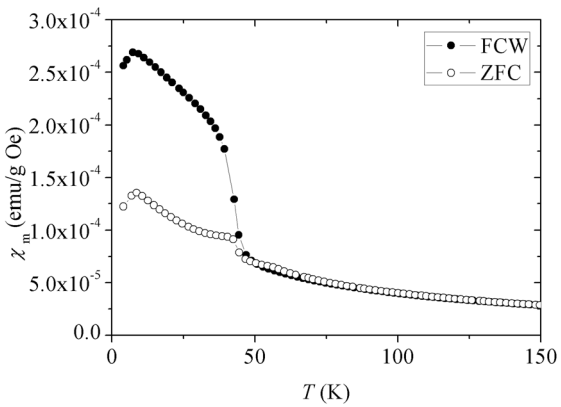

Fig. 1 ZFC and FC curves measured by applying H = 50 Oe in the temperature range 4–300 K; two critical temperatures can be identified, T_1 = 9 K and T_2 = 44 K. Between 150 K and 300 K the curves are perfectly superimposed.

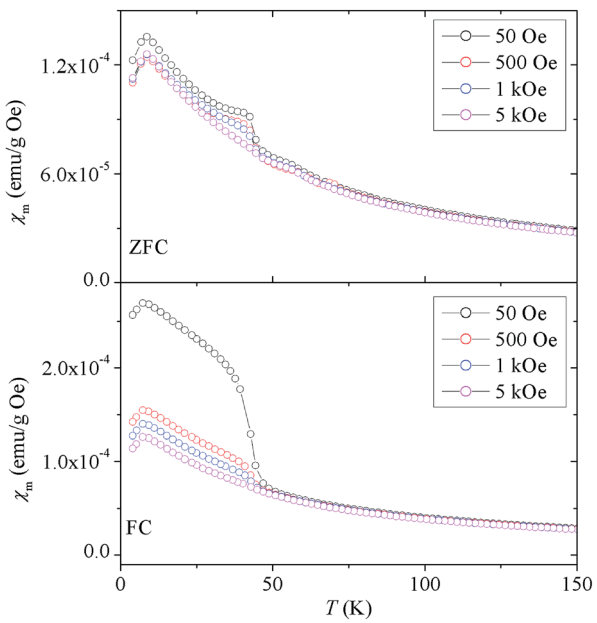

Fig. 2 Field dependence of the ZFC (upper panel) and FC (lower panel) curves measured with different applied fields. Between 150 K and 300 K the curves are perfectly superimposed.

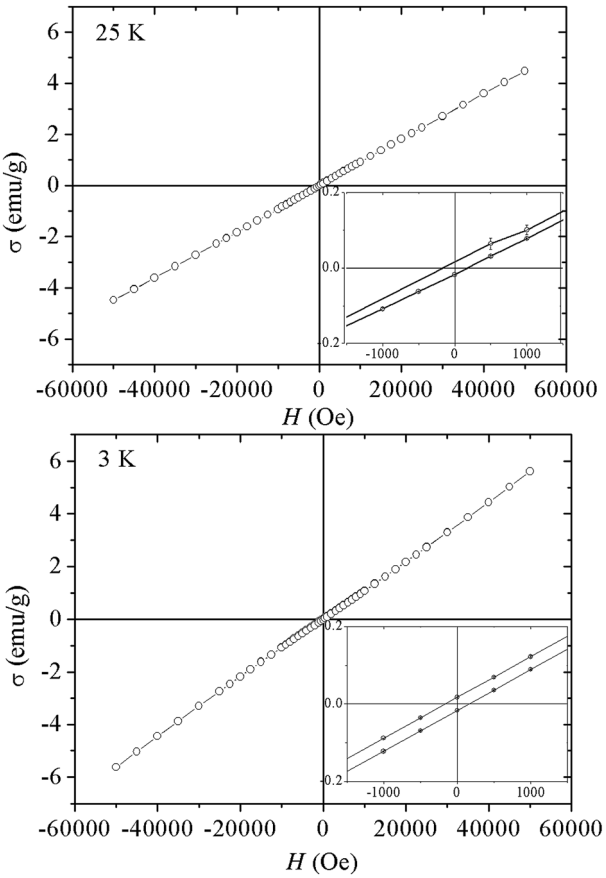

Fig. 3 Hysteresis loops measured at 25 K (top) and 3 K (bottom); a small coercive field, of the order of $H_c = 160$ Oe, is present at both temperatures as shown in the insets.

$c = 2\sqrt{2}a_p$. On the basis of the collected neutron diffraction data the symmetry of this polar structure is retained down to 2 K and no antisite defects or atom vacancies were detected during the refinement. As shown in Fig. 4 some additional reflections, that can be indexed with a propagation vector $\kappa = [1/4\ 0\ 0]$, appear below 10 K; the relation with the second critical temperature observed in the magnetization measurements suggests that their magnetic nature is attributable to long range ordering. In contrast no additional reflections appear below the first magnetic transition at 44 K, where only an additional diffuse scattering that could be indicative of a short range ordering is observed (Fig. 4, inset). It is interesting to note that the profile shape of the diffuse scattering does not follow the characteristics of a Warren type function,[10] suggesting a 3D nature of the short range ordering. The broad diffuse peak was, after the subtraction of the background, fitted with a Gaussian function to obtain an indication on the average magnetic correlation length, calculated as 19(1) Å by the Scherrer formula ($K = 0.9$) applied to the fitted profile.

The magnetic structure analysis was carried out with the superspace formalism.[1] This approach, originally developed for the structure analysis of aperiodic crystals, can also be applied to the study of an incommensurate magnetic structure, as evidenced by a few examples recently published in the literature.[2–5]

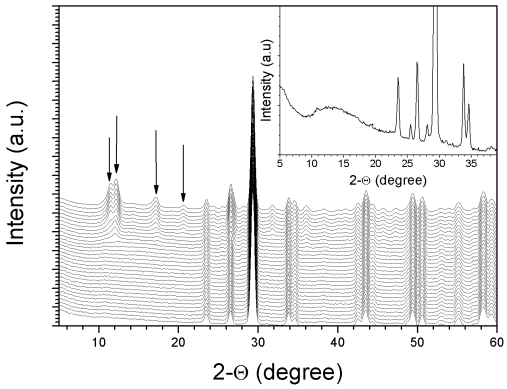

Fig. 4 Neutron powder data in temperature obtained at the D20 line with $\lambda = 2.41$ Å, the arrows indicate the magnetic reflection. (Inset) Zoom of the low angle region of the 10 K diffraction pattern in which the diffuse scattering is clearly visible.

In the superspace formalism a magnetic structure is described by a conventional structure related to the nuclear fundamental cell associated with a series of magnetic modulation functions, with propagation vector κ, that describe the variation of the momentum from the basic structure.[7,11] The basic magnetic structure is described by its magnetic space group derived from the coloured Shubnikov groups[12] and is at the same time related to the paramagnetic nuclear space group. The magnetization of the j-th atom in the unit cell is therefore defined by the value on the basic structure $M_{j,0}$ and from a modulation function $M_j(x_4 = t + k\cdot r_{l,j})$ in which x_4 is the so-called internal coordinate and $r_{l,j}$ indicates the position of the j-th atom of the basic structure in the l-th unit cell. Consequently it is represented as a (3 + 1)-dimensional space in which the additional dimension refers to the internal coordinate. The modulation function can be expressed in a Fourier series:

$$\vec{M}_j\left(\vec{k}\cdot\vec{r}_{l,j}\right) = \vec{M}_{j,0} + \sum_{n=1}^{\infty}\left[\vec{M}_{j,ns}\sin\left(2\pi n\vec{k}\cdot\vec{r}_{l,j}\right) + \vec{M}_{j,nc}\cos\left(2\pi n\vec{k}\cdot\vec{r}_{l,j}\right)\right] \quad (1)$$

Analogous to nuclear aperiodic crystals, the modulation waves are conformed to symmetry constraints imposed by the magnetic superspace group.

The analysis of the pure magnetic diffraction pattern, obtained from subtraction of the pattern collected at 2 and 10 K, pointed out two main fundamental aspects: (i) the magnetic scattering corresponding to nuclear reflections, indicates that the M_0 terms differ from zero and (ii) the systematic absence of $00l$ reflections with $l = 2n$. By consulting the Bilbao crystallographic server[13–15] and in particular the program MAGNTEX[16] the possible space groups of the basic magnetic structure were found to be $Pmc2_1$ (Fedorov group) or alternatively $Pm'c'2_1$. The combination between these two space groups with the propagation vector produce four possible superspace groups that are: $Pmc2_1(\alpha 00)000$, $Pmc2_1(\alpha 00)0s0$, $Pm'c'2_1(\alpha 00)000$, and $Pm'c'2_1(\alpha 00)0s0$.

Table 1 Crystal data and refinement parameters at 2 K

Chemical formula			Pb_2MnWO_6
Superspace magnetic group			$Pmc2_1(\alpha 00)0s0$
a (Å)			8.01620(11)
b (Å)			5.78216(8)
c (Å)			11.63487(9)
α			0.25
V (Å^3)			541.10(16)
Z			4
	D2B		D20
λ (Å)	1.594		2.41
GOF	1.68		5.92
R_p	5.54%		2.28%
$_wR_p$	6.98%		3.26%
Overall GOF		3.41	
Overall R_p		2.37%	
Overall $_wR_p$		3.51%	

The Rietveld refinement was attempted in all possible superspace groups but a reasonable solution was found only in the case of $Pmc2_1(\alpha 00)0s0$ (Table 1). In this group two independent manganese sites, of the basic nuclear cell, lie on the mirror plane, forcing the magnetic moment of the basic structure

Table 2 Definition of modulation functions for the magnetic moment of the manganese atoms

Site	Magnetization expression
Mn1	$M_{x,0} + M_{y,c}\cos(2\pi x_4) + M_{z,c}\cos(2\pi x_4)$
Mn2	$M_{x,0} + M_{y,c}\cos(2\pi x_4) + M_{z,c}\cos(2\pi x_4)$

Table 3 The atoms position and magnetic parameters of the structure at 2 K

Site	X	Y	Z	U_{iso}
Pb1	0.7628(9)	0.9746(16)	0.8653(11)	0.015(2)
Pb2	0.7462(11)	0.5477(12)	0.5786(11)	0.011(2)
W1	0	0.522(4)	0.8644(12)	0.020(5)
W2	0.5	0.001(5)	0.6117(12)	0.018(5)
Mn1	0.5	0.492(6)	0.8646(16)	0.006(6)
Mn2	0	0.998(7)	0.1027(15)	0.011(6)
O1	0	0.724(3)	0.730(2)	0.0159(5)
O2	0	0.311(3)	0.973(2)	0.0159(5)
O3	0.5	0.767(4)	0.7103(18)	0.0159(5)
O4	0.5	0.222(3)	0.721(2)	0.0159(5)
O5	0	0.249(3)	0.7442(13)	0.0159(5)
O6	0.5	0.209(3)	0.477(3)	0.0159(5)
O7	0.7384(15)	0.0361(16)	0.5956(12)	0.0159(5)
O8	0.5	0.294(4)	0.9958(16)	0.0159(5)
O9	0.7667(15)	0.520(2)	0.8655(12)	0.0159(5)
O10	0	0.786(4)	0.9568(17)	0.0159(5)

Site	$M_{x,0}$	$M_{y,c}$	$M_{z,c}$
Mn1	−2.31(3)	−3.26(15)	1.57(7)
Mn2	2.31(3)	5.06(13)	1.57(7)

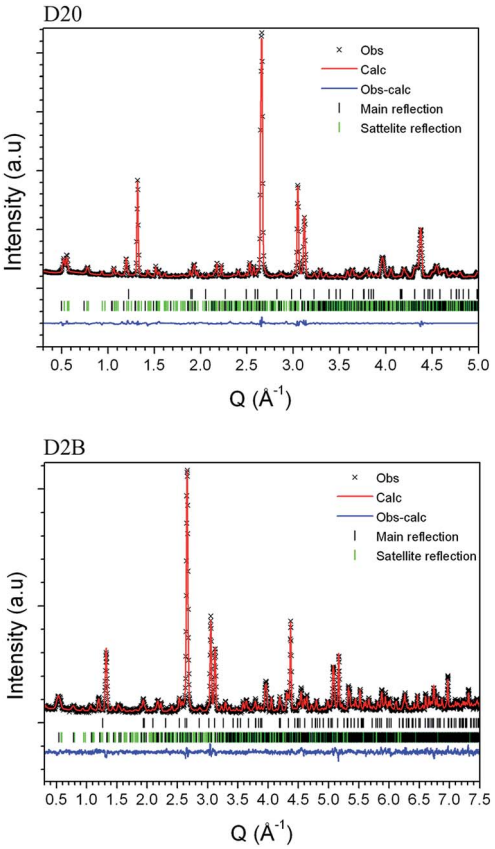

Fig. 5 Rietveld refinement of the neutron powder diffraction data taken at 2 K on D20 (top) and D2B (bottom) using the nuclear and magnetic structure models as described in the text. Observed (black crosses), calculated (red line) and difference (blue line) pattern. The tick marks indicate the calculated position of the main phase (bottom) and secondary phase $PbWO_4$ (top, present in less than 5%).

along the a axis. Owing to the presence in the diffraction pattern of only first order satellites, the symmetry permitted terms of the Fourier series, as reported in Table 2, were truncated at $n = 1$. Further constraints were introduced as suggested, during the refinement, by the behaviour of the refined parameters: the $M_{x,s}$ terms having negligible values within the e.s.d.'s, were imposed to zero in the last refinement cycles, whereas the $M_{x,0}$ and $M_{z,c}$ terms of the two independent sites were forced to assume the same modulus and opposite sign as indicated by the Rietveld model approaching the convergence.

The nuclear and magnetic atomic parameters at 2 K, obtained from the simultaneous refinement of the D2B and D20 data, are reported in Table 3 and the corresponding Rietveld plots are shown in Fig. 5. To further confirm the magnetic structure, the resulting model was used to refine the pure magnetic pattern obtained from the subtraction between the 2 K and 10 K patterns at the D20 line. The agreement between the observed and the calculated pattern is satisfactory ($_wR_B = 9\%$), as shown in the Rietveld plot of Fig. 6.

In the superspace formalism the 3D structure is reconstructed by a t-section of the (3 + 1)D space perpendicular to the

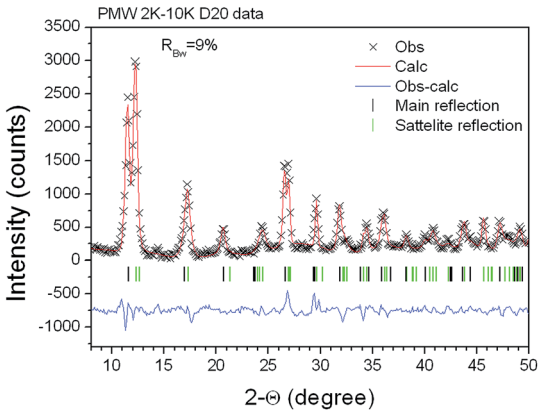

Fig. 6 Rietveld refinement of the pure magnetic diffraction pattern obtained by subtraction of the 2 K and 10 K data.

3D space, in which the magnetic moment components along the fourth axis of the (3 + 1)D space are obtained by the relation:

$$M_{l,j}(x_4) = M_{l,j}(t + \vec{k}\cdot\vec{r}_{l,j}) \quad (2)$$

whereas in the case of an incommensurate structure any t-section is equivalent to the others,[7] the commensurate case requires particular attention, since different choices can give rise to different symmetries for the 3D superstructure. In fact for a commensurate superstructure the x_4 coordinate assumes only a discrete number of values (4 in the present case) limiting the possible positions of Mn atoms in the t-plot (Fig. 7). In fact in the case of a N_s-fold commensurate structure the t-section with $t = n/N_s - t_0$, where n =(0, 1, and N_s−1) and t_0 is the origin choice for the t-section, gives equal descriptions of the structure. In this frame in defining the N_s-fold superstructure the choice of the t_0 parameter can give different magnetic components and even different magnetic space groups. Among the possible t_0 sets, both the conditions $t_0 = 0 + n/4$ and $t_0 = 1/8 + n/4$ give rise to superstructures with orthorhombic $Pmn2_1$ magnetic symmetry whereas any other value of t_0, defines a superstructure with monoclinic Pn magnetic symmetry. The solution with $t_0 = 0 + n/4$ leads to a magnetic total momentum $|M| = 5.73\ \mu_B$ exceeding what is expected for Mn^{2+} at 2 K and therefore it has been be rejected. In contrast $t_0 = 1/8 + n/4$ represents the most convenient solution, not only for symmetry reasons, but also for plausible values of the unconstrained magnetic moments that are similar to each other as shown in Table 4. The commensurate fourth-fold superstructure is shown in Fig. 8. The structure is constituted by blocks separated by mirror planes perpendicular to the a axis producing the inversion of the M_y component sign; the manganese atoms lying on the mirror plane are constrained by the symmetry to assume a magnetic moment collinear to the a axis. In the ac plane (see Fig. 8 bottom) the magnetic interaction gives rise to zig-zag chains of FM alignments (blues straight lines), stacked along the c axis with AF coupling (green straight lines) as expected from the magnetization measurement.

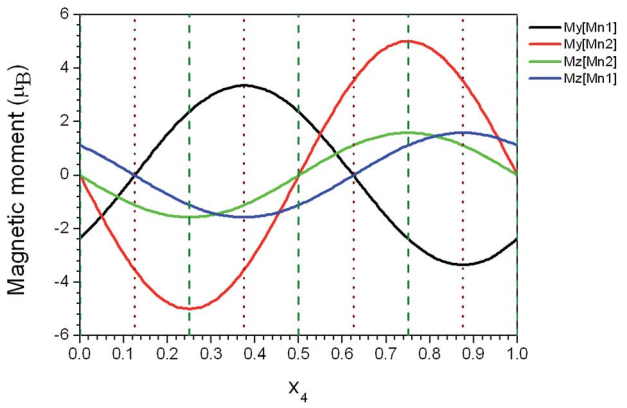

Fig. 7 Representation of the magnetic moment value along the fourth axis of the (3 + 1)D space of the 2 K refinement. The dashed and the dotted lines represent the position of the manganese atoms with the different choice of the t section, respectively, t_0 = 0 and 1/8. The position of the manganese atoms in the t-space are obtained from $t_{l,j} = t_0 + k\cdot r_{l,j}$ (see text).

Table 4 Value of the magnetic moment for each atom in the fourfold superstructure with t_0 = 1/8. The atoms label, according to Table 3, indicates the position in the nuclear unit cell

Atom	x_4	M_x	M_y	M_z	$\|M\|$
Mn1	0	2.306(29)	0.000(0)	0.000(0)	2.306(29)
Mn1	0.25	2.306(29)	3.193(154)	−1.580(71)	4.244(172)
Mn1	0.5	2.306(29)	0.000(0)	0.000(0)	2.306(29)
Mn1	0.75	2.306(29)	3.193(154)	1.580(71)	4.244(172)
Mn2	0	2.306(29)	−3.614(65)	1.117(50)	4.430(88)
Mn2	0.25	2.306(29)	3.614(65)	1.117(50)	4.430(88)
Mn2	0.5	2.306(29)	−3.614(65)	1.117(50)	4.430(88)
Mn2	0.75	2.306(29)	3.614(65)	1.117(50)	4.430(88)

The analysis of magnetic scattering in the neutron diffraction data taken on increasing the temperature reveals interesting features. On one side, different from the satellite reflections whose intensity vanishes around 10 K in agreement

Table 5 Rietveld refinement parameters of the incommensurate magnetic structure at 7.9 K

Chemical formula	Pb_2MnWO_6
Superspace magnetic group	$Pmc2_11'(\alpha00)0s0s$
a (Å)	8.0206(8)
b (Å)	5.7813(8)
c (Å)	11.6316(18)
α	0.230(7)
V (Å^3)	539.36(16)
Z	4
GOF	1.67
R_P	8.97%
$_wR_P$	11%
Magnetic parameters	
$M_{y,c}$	$M_{z,c}$
2.11(5)	1.99(8)

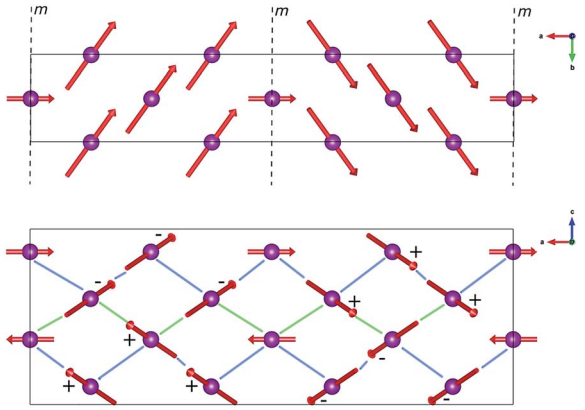

Fig. 8 Projection of the proposed magnetic model in the *ab* plane (top) and *ac* plane (bottom), the blue line indicates a ferromagnetic interaction of the M_x component and the green line indicates an antiferromagnetic interaction. The + and − symbols indicate the direction of the out of plane component of the magnetic moment.

with the magnetization behaviour, the magnetic contribution to the intensity on the fundamental reflections disappears above 7 K. On the other side the progressive shift of the satellite reflections suggests a thermal evolution of the propagation vector that involves a reduction of the *a* component. Fig. 9 displays the discrepancy of the refined propagation vector from the commensurate value obtained at 2 K as a function of the temperature. The propagation vector becomes clearly incommensurate above 7 K, where the magnetic intensity on the fundamental reflection disappears suggesting the presence of a magnetic phase transition at this temperature.

The incommensurate magnetic structure was solved from the powder neutron diffraction pattern collected at 8 K. Owing to the absence of magnetic intensity on the fundamental reflections, the Shubnikov symmetry of the basic magnetic structure univocally corresponds to the grey space group $Pmc2_11'$. It follows that the two possible magnetic super-space groups are $Pmc2_11'(a00)0s0s$ and $Pmc2_11'(a00)000s$. Because of the limited number of magnetic reflections, the Rietveld refinement was performed on the pure magnetic diffraction

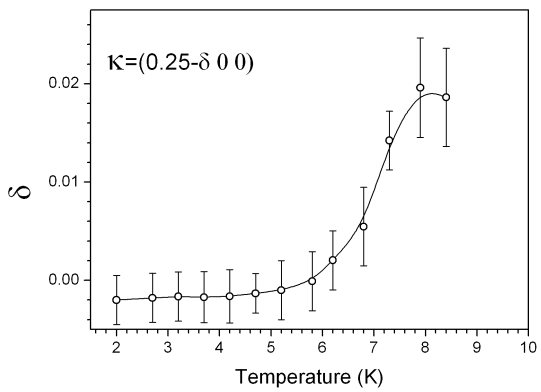

Fig. 9 Thermal evolution of the propagation vector in terms of its deviation from the commensurate value.

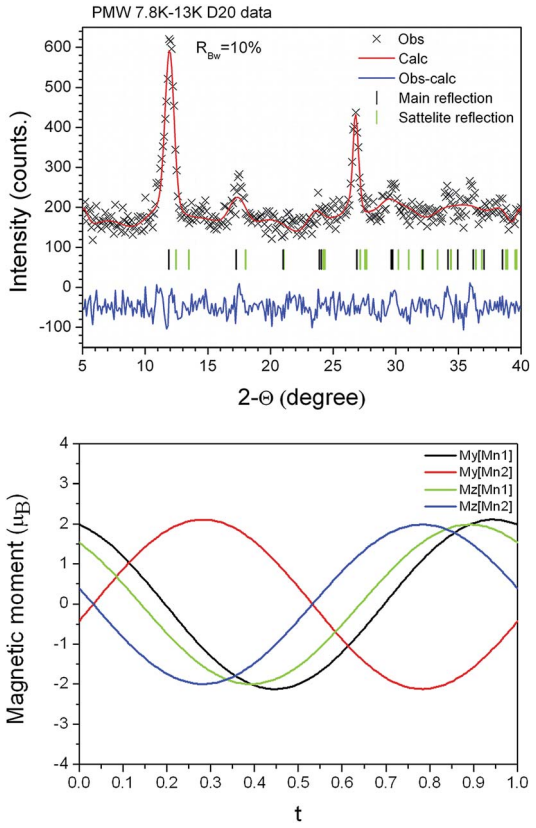

Fig. 10 Top) Rietveld refinement of the incommensurate magnetic structure at 7.9 K on the pure magnetic diffraction pattern obtained from the subtraction between the 7.9 K and 13 K diffraction patterns. (Bottom) the *t*-plot of the incommensurate magnetic structure at 7.9 K.

pattern obtained by the subtraction of the 13 K pattern from the 8 K one. Also in this case some constraints on the Fourier amplitudes of the two Mn sites were introduced to stabilize the refinement; in particular, by taking into account the values obtained from the last cycles of refinement the $M_{y,c}$ terms of the two independent sites, were constrained to exhibit AF configuration, whereas the $M_{z,c}$ terms were imposed to be equivalent. The best agreement factor was obtained from the $Pmc2_11'(a00)0s0s$ space groups (Table 5) and the Rietveld plot is shown in Fig. 10 with the resultant *t*-plot.

In this case, thanks to the incommensurate character of the magnetic structure, any choice of t_0 gives rise to analogue magnetic structures in which the Mn moments lie in the *bc* plane with resultant *moduli* varying with a wave-like fashion along the *a* axis as schematically represented in Fig. 11.

The determination of the two magnetic models at 2 K and 8 K made it possible to refine all the diffraction patterns and to follow the thermal evolution of the magnetic ordering at low temperatures by considering M_x the moment arising from the basic magnetic structure and $M_{y,z}$, calculated as $M_{yz} = \sqrt{M_{y,c}^2 + M_{z,c}^2}$, as the one connected to the modulated part of the magnetic structure. The data obtained from the two independent Mn sites were averaged and fitted with a classical power law

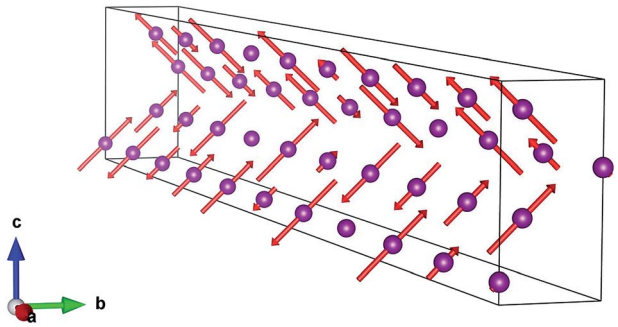

Fig. 11 3D view of the first 10 cells along the *a* axis for the incommensurate structure at 7.9 K.

$$M(T) = M_0\left(1 - \frac{T}{T_c}\right)^{\beta} \quad (3)$$

in order to obtain the critical exponent of the magnetic transitions and the extrapolated moment of the manganese atoms at 0 K. The fittings, reported in Fig. 12, were extended also to the total magnetic moment, that resulted to be close to the expected value for Mn(II) atoms in the *hs* configuration, with a critical exponent β conforming to the classical model of a 3D Heisenberg magnet.[17] The analysis of the single components allows a better comprehension of the complex magnetic transition. At first, below 10 K, the magnetic ordering develops in the *bc* plane and involves an incommensurate modulation of the Mn moments along the *a* axis. By decreasing the temperature the magnetic propagation vector changes its periodicity and turns commensurate around 7 K in correspondence to the appearance of the magnetic moment component along the *a* axis.

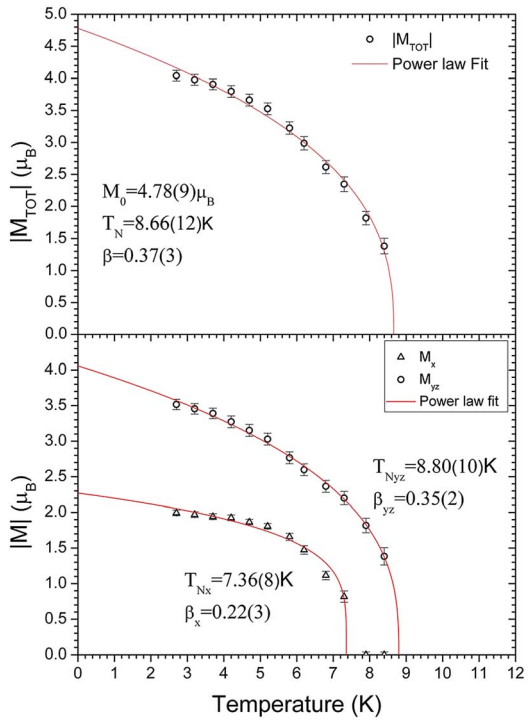

Fig. 12 Thermal evolution of the refined average magnetic moment of the Mn atoms in the magnetic structure. The red line indicates the fitting with a classical power law (see text).

Discussion

On the basis of the performed characterizations the system undergoes, by decreasing the temperature, two magnetic transitions at $T_1 = 44$ K and $T_2 = 9$ K. The transitions reveal an antiferromagnetic nature, with a moderate ferromagnetism evidenced by the irreversibility between ZFC and FC in $M(T)$ measurements and by a narrow coercive field detected in $M(H)$ measurements between and below the critical temperatures. The magnetic behaviour observed for PMW is similar to those reported for A_2MnWO_6 (A = Ca, Sr, and Ba),[18–20] involving comparable transition temperatures and similar features of the magnetization. The first transition, occurring at T_1, is associated with short-range ordering, as evidenced by the appearance in neutron diffraction of diffuse scattering below 44 K. By further cooling the system undergoes a second magnetic transition leading to an incommensurate modulated structure that evolves to a commensurate one; the incommensurate–commensurate (IC-C) transition is related to the appearing of a magnetic moment component along the *a* axis which is described within the nuclear unit cell and has consequently no modulated character. The IC-C transition can be expressed in terms of super-space symmetry and consists in removing the symmetry operator $(1'|0\ 0\ 0\ 1/2)$, indicated in Seitz notation, from the $Pmc2_11'(a00)0s0s$ space group, and by the lock-in of the propagation vector to the commensurate periodicity.

The transition occurring at T_2 is associated with a magnetostrictive effect particularly evident along the *c* polar axis of the $Pmc2_1$ space group, as shown in Fig. 13. The indication of a spin lattice coupling along this axis, corresponding to the polar direction of the crystal, reasonably suggests a magneto(di) electric coupling in this system. Moreover it is interesting to note that, different from the T_1 transition that likely shows a second order character in the limit of the resolution of the analysed diffraction data, a sudden increase of the *c* cell parameter is observed indicating a possible first order character of the transition.

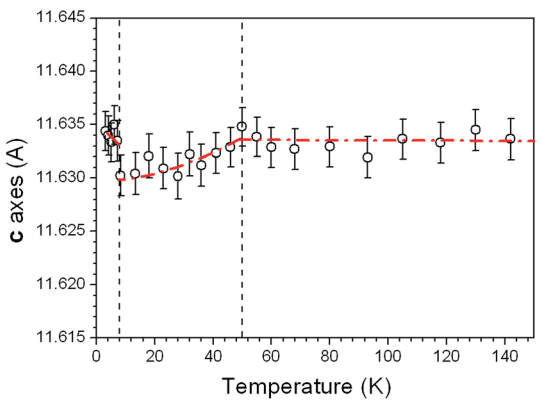

Fig. 13 magnetostriction effect on the *c* axis of the PMW structure.

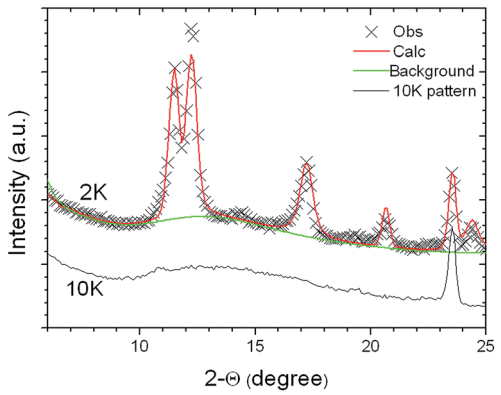

Fig. 14 low angle Rietveld plot of the D20 diffraction pattern at 2 K. The green line indicates the refined background that shows the same diffuse scatter seen in the diffraction pattern obtained at 10 K (shown for comparison).

A further interesting phenomenon is represented by the persistence of the diffuse scattering, attributed to short-range ordering, even below the second magnetic transition, as pointed out by the comparison, in Fig. 14, of the background of the Rietveld plot of the refined 2 K data with the corresponding 10 K diffraction pattern. The persistence of the diffuse scattering after the rise of the magnetic diffraction peaks, related to long-range ordering, suggests a different nature of the two phenomena. The most plausible explanation is given by the presence of anti-phase boundaries generating AF exchange paths with higher T_c but limited spatial distribution ranging the observed correlation length (19 Å) in the polycrystalline sample. It is widely recognized that this type of defects frequently observed in double perovskite systems has a direct influence on magnetic properties.[21,22] Given the small spatial extension of these domains the AF sublattices are not completely balanced giving rise to a weak ferromagnetic contribution that reaches saturation at low applied fields. Conversely in the case of higher applied fields this contribution is masked by the linear response of the AF structure (see Fig. 2). This structural defect can reasonably be the origin of the observed weak FM evidenced in magnetization curves shown in Fig. 1.

Conclusions

In this paper we describe the complex magnetic behaviour of the multiferroic double perovskite Pb_2MnWO_6. This system exhibits two main magnetic transitions whose evolution is observed in a limited temperature range. The first one, occurring at 44 K, is characterized by a short-range order which is converted to an incommensurate long range magnetic structure at 9 K having the superspace group $Pmc2_11'(\alpha 00)0s0s$. Thus, by lowering the temperature down to 6 K, the system undergoes to the magnetic ground state showing commensurate propagation vector $\kappa = (1/4\ 0\ 0)$ and symmetry $Pmc2_1(\alpha 00)0s0$. The IC-C switching implies the removal of the $(1'|0\ 0\ 0\ 1/2)$ symmetry element, allowing the rise up of the magnetization along the a axis and the lock-in of the propagation vector to (1/4 0 0).

The complex magnetic behaviour of the PMW system and the peculiar evolution of its magnetic structure represent an important test for the general application of the superspace formalism to magnetic structure solution and refinement. The results demonstrate that the superspace approach can be considered as a powerful tool, not only in the case of the incommensurate modulated structure, representing its natural target, but also in the case of the complex commensurate structure, being able to reduce the number of variables required and to stabilize the refinement procedure. Moreover the superspace approach results particularly valuable for the treatment of the IC-C magnetic transitions.

It is important to stress out that the application of superspace can be of pivotal importance in the investigation of magneto–electric coupled systems since the magnetic symmetry and its temperature dependence are fundamental in the study of spin–lattice interactions.

As demonstrated in the PMW case, this approach not only allows to face magnetic modulation independently from its commensurability, but can explain the magnetic transition in terms of simple symmetry changing, as it is usually described in conventional solid state transformations.

Acknowledgements

One of the authors (Fabio Orlandi) thanks Fondazione Cariparma for financial support. F.O. thanks Dr Francesco Mezzadri for the helpful discussion and Dr Davide Calestani for his assistance with thermal treatment procedures.

Notes and references

1 A. Janner and T. Janssen, *Acta Crystallogr., Sect. A: Cryst. Phys., Diffr., Theor. Gen. Crystallogr.*, 1980, **36**, 399.
2 I. Urcelay-Olabarria, J. M. Perez-Mato, J. L. Ribeiro, J. L. Garcia-Munoz, E. Ressouche, V. Skumryev and A. A. Mukhin, *Phys. Rev. B: Condens. Matter Mater. Phys.*, 2013, **87**, 014419.
3 A. M. Abakumov, A. A. Tsirlin, J. M. Perez-Mato, V. Petříček, H. Rosner, T. Yangand and M. Greenblatt, *Phys. Rev. B: Condens. Matter Mater. Phys.*, 2011, **83**, 214402.
4 W. Slawinski, R. Przenioslo, I. Sosnowska and V. Petrícek, *Acta Crystallogr., Sect. B: Struct. Sci.*, 2012, **68**, 240.
5 J. L. Ribeiro and J. M. Perez-Mato, *J. Phys.: Condens. Matter*, 2011, **23**, 446003.
6 V. Petricek, M. Dusek and L. Palatinus, *Z. Kristallogr.*, 2014, **229**, 345.
7 J. M. Perez-Mato, J. L. Ribeiro, V. Petricek and M. I. Aroyo, *J. Phys.: Condens. Matter*, 2012, **24**, 163201.
8 F. Orlandi, L. Righi, R. Cabassi, D. Delmonte, C. Pernechele, F. Bolzoni, F. Mezzadri, M. Solzi, M. Merlini and G. Calestani, *Inorg. Chem.*, 2014, DOI: 10.1021/ic501328s.
9 J. Blasco, R. I. Merino, J. García and M. C. Sánchez, *J. Phys.: Condens. Matter*, 2006, **18**, 2261.
10 B. E. Warren, *Phys. Rev.*, 1941, **59**, 693.
11 V. Petrícek, J. Fuksa and M. Dusek, *Acta Cryst.*, 2010, **A66**, 649.

12 D. B. Litvin, *Acta Crystallogr., Sect. A: Found. Crystallogr.*, 2008, **64**, 419.
13 M. I. Aroyo, J. M. Perez-Mato, D. Orobengoa, E. Tasci, G. de la Flor and A. Kirov, *Bulg. Chem. Commun.*, 2011, **43**(2), 183.
14 M. I. Aroyo, J. M. Perez-Mato, C. Capillas, E. Kroumova, S. Ivantchev, G. Madariaga, A. Kirov and H. Wondratschek, *Z. Kristallogr.*, 2006, **221**, 15.
15 M. I. Aroyo, A. Kirov, C. Capillas, J. M. Perez-Mato and H. Wondratschek, *Acta Crystallogr., Sect. A: Found. Crystallogr.*, 2006, **62**, 115.
16 S. V. Gallego, E. S. Tasci, G. de la Flor, J. M. Perez-Mato and M. I. Aroyo, *J. Appl. Crystallogr.*, 2012, **45**, 1236.
17 C. Holm and W. Janke, *Phys. Rev. B: Condens. Matter Mater. Phys.*, 1993, **48**, 936.
18 A. K. Azad, S. A. Ivanov, S. G. Eriksson, J. Eriksen, H. Rundlöf, R. Mathieu and P. Svedlindh, *Mater. Res. Bull.*, 2001, **36**, 2485.
19 A. K. Azad, S. Ivanov, S. G. Eriksson, J. Eriksen, H. Rundlöf, R. Mathieu and P. Svedlindh, *J. Magn. Magn. Mater.*, 2001, **237**, 124.
20 A. K. Azad, S. Ivanov, S. G. Eriksson, H. Rundlöf, J. Eriksen, R. Mathieu and P. Svedlindh, *Mater. Res. Bull.*, 2001, **36**, 2215.
21 R. I. Dass and J. B. Goodenough, *Phys. Rev. B: Condens. Matter Mater. Phys.*, 2003, **67**, 014401.
22 J. B. Goodenough and R. I. Dass, *Int. J. Inorg. Mater.*, 2000, **2**, 3.